The metallicity spread and the age-metallicity relation of ω Centauri [1]

S. Villanova and D. Geisler
Departamento de Astronomia, Casilla 160, Universidad de Concepcion, Chile
svillanova@astro-udec.cl

R.G. Gratton
INAF - Osservatorio Astronomico di Padova, Vicolo dellOsservatorio 5, 35122 Padova, Italy
and

S. Cassisi
INAF - Ossservatorio Astronomico di Teramo, via M. Maggini, 64100 Teramo, Italy

ABSTRACT

ω Centauri is a peculiar Globular Cluster formed by a complex stellar population. To shed light on this, we studied 172 stars belonging to the 5 SGBs that we can identify in our photometry, in order to measure their [Fe/H] content as well as estimate their age dispersion and the age-metallicity relation. The first important result is that all of these SGBs has a distribution in metallicity with a spread that exceeds the observational errors and typically displays several peaks that indicate the presence of several sub-populations. We were able to identified at least 6 of them based on their mean [Fe/H] content. These metallicity-based sub-populations are seen to varying extents in each of the 5 SGBs.

Taking advantage of the age-sensitivity of the SGB we showed that, first of all, at least half of the sub-populations have an age spread of at least 2 Gyrs. Then we obtained an age-metallicity relation that is the most complete up to date for this cluster.

The interpretation of the age-metallicity relation is not straightforward, but it is possible that the cluster (or what we can call its progenitor) was initially composed of two populations having different metallicities. Because of their age, it is very unlikely that the most metal-rich derives from the most metal-poor by some kind of chemical evolution process, so they must be assumed as two independent primordial objects or perhaps two separate parts of a single larger object, that merged in the past to form the present-day cluster.

Subject headings: globular clusters: general — globular clusters: individual(NGC 5139)

1. Introduction

Omega Centauri is a fascinating and enigmatic object: it appears to be a globular cluster (GC), but it has a very complex stellar population, and with its unusual mass ($M \sim 3 \times 10^6 M_\odot$) it has often been suggested to be the remains of a larger stellar system. It has received a large amount of attention; for a review see Meylan (2003). One of the most interesting results (Bedin et al. 2004) was the discovery that over a range of at least two magnitudes the main sequence splits into red and blue branches. Follow-up spectroscopic studies at medium resolution led to the finding that,

[1] Based on FLAMES+GIRAFFE@VLT observations under the program 082.D-0424(A)

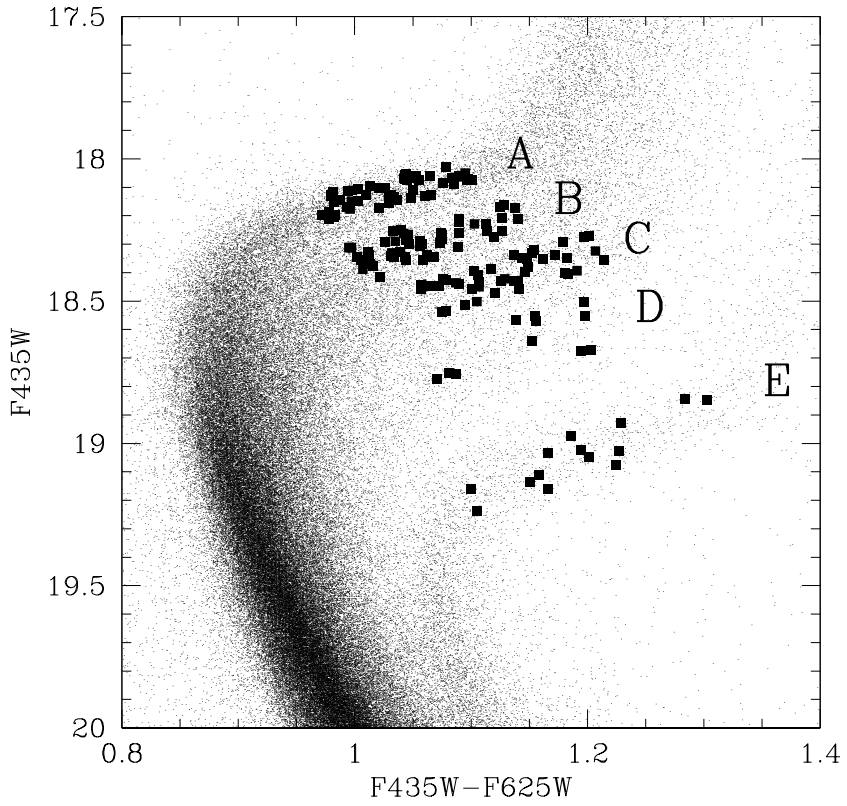

Fig. 1.— SGB region of ω Cen with the 5 branches identified in HST data (Villanova et al. 2007) and the target stars indicated.

contrary to any expectation from canonical stellar models, the bluer branch of the MS is more metal-rich than the red (Piotto et al. 2005). At the moment, the only explanation of the photometric and spectroscopic properties of the double main sequence that is at all plausible is that the bluer branch of the MS has an unusually high helium content (Norris 2004; King et. al. 2012).

It has been suggested that this unusual He-rich population might come from material contaminated by the ejecta of massive ($25 M_{\odot}$, Norris 2004), or slightly less massive (10–14 $M_{\odot}$, Piotto et al. 2005) supernovae, or from rapidly rotating low-metallicity massive stars (Maeder & Meynet 2006), or from intermediate-mass asymptotic-giant-branch stars (Izzard et al. 2004).

This double MS was not totally unexpected because Norris et al. (1996) found a bimodal distribution of [Ca/H] for RGB stars based on low-resolution spectra, with a first peak at [Ca/H]$\sim$-1.4 and a second peak at [Ca/H]$\sim$-1.0. This result was partially confirmed in the same period by Suntzeff & Kraft (1996) that, using the Calcium triplet method, found a [Fe/H] distribution with a peak at [Fe/H]$\sim$-1.7 and a tail toward higher metallicities.

However Omega Centauri is much more complex than that, because more than two stellar populations are present. Sollima et al. (2005) could identify at least 4 stellar populations on the sub-giant branch (SGB) having a mean [Fe/H]=-1.7,-1.3,-1.0, and -0.6 dex respectively, based on CaT abundances. Villanova et al. (2007) identified photometrically at least five stellar populations in the SGB region, and spectroscopically

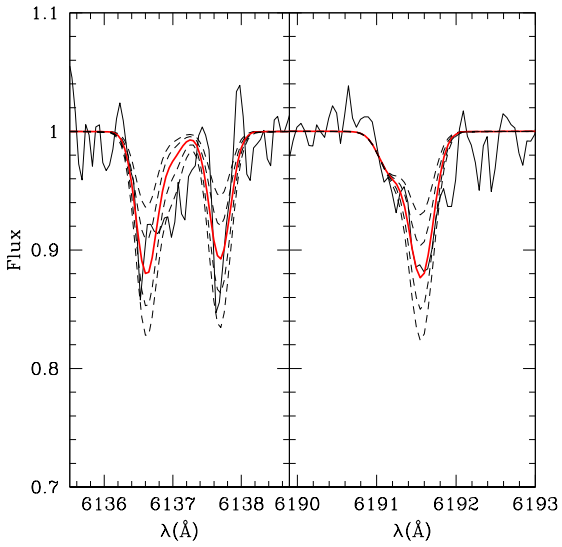

Fig. 2.— Comparison between the spectrum of the star SGB_B.12 ([Fe/H]=-1.80) and 5 synthetic spectra having [Fe/H]=-2.30,-2.05,-1.80,-1.55, and -1.30. The best fitting spectrum is indicated with a thick red line.The star has F435W=18.4 and S/N=35, typical of the sample.

three populations based on their iron content, at [Fe/H]=-1.68, -1.37, and -1.14.

Several other studies tried to establish the number and iron content of the populations. The first was Calamida et al. (2009), based on Strömgren photometry of the red-giant branch (RGB). The authors found 6 peaks in the iron distribution at [Fe/H]=-1.73,-1.29,-1.05,-0.80,-0.42, and -0.07 dex. On the other hand Johnson & Pilachowski (2010), based on a metallicity distribution obtained by a large number of high resolution RGB spectra, identified four groups at [Fe/H]=-1.75,-1.50,-1.10,-0.75 dex. Recently Pancino et al. (2011) suggested also the presence of a very metal poor population, at [Fe/H]=-1.95, based on high-resolution spectra.

Finally Marino et al. (2011) found that their metallicity distribution is consistent with the presence of multiple peaks corresponding to [Fe/H]=-1.75,-1.60, -1.45,-1.00, a broad distribution of stars extending between -1.40 and -1.00, and a tail of metal-rich stars reaching values of [Fe/H]-0.70.

In addition Stanford et al. (2006) found that an age range of 2-4 Gyrs exists in the cluster, based on the position and metallicity of stars in the TO-SGB region. This result was confirmed by Villanova et al. (2007), who also suggested that a large age-spread could affect the cluster. In particular they found that stars that belong to the most metal-poor group ([Fe/H]∼-1.7) span an age-range of several Gyrs and that surprisingly the most metal-rich component is also the oldest.

After this brief summary it is clear that a more complete study is required in order to better determine the number and mean metallicity of subpopulations in ω Cen and its age-metallicity relation. This is the best way to understand the complex star-formation history of this intriguing object. Such a study must be cafeful to try and account for any possible spread in He and CNO that affect the stars of the cluster, as found Norris (2004) and Marino et al. (2011).

The best region in the CMD for this purpose is the SGB, where the position of a star strongly depends not only on the metallicity, but also on the age. In this way both age and metallicity can be used to disentangle and identify the subpopulations as well as to study any possible age-spread and age-metallicity relation affecting them.

For this purpose we collected a large spectroscopic database that covers the entire SGB of the central HST photometric field (see Villanova et al. 2007).

In Section 2 we present the observations and data reduction. In Section 3 we discuss the abundance measurements, while Section 4 presents the results. In Sections 5 our findings are compared with the results from the literature. Finally Section 6 discusses the implications of the observational facts presented in this paper for the stellar populations in ω Centauri, the age spread, the age-metallicity relation, and the origin of this anomalous cluster.

2. Observations and data reduction

The spectroscopic data come from the ESO proposal 082.D-0424(A), and were collected in January–March 2009 with FLAMES@VLT+GIRAFFE. The sky was clear, and the typical seeing was ∼0.8 arcsec (FWHM). We used the MEDUSA mode, which obtains 132 spectra simultaneously. To have enough S/N and spectral resolution we

used the HR13 set-up, which gives $R = 22500$ in the 6120–6405 Å range.

The main target was the SGB, where we pointed 450 stars divided in 7 placements and observed 4 or 5 hours each. The remaining fibers were placed on HB (∼270) and RGB (∼80) stars and on the sky (10 fibers for each plate). Results for the RGB targets were already presented in Marino et al. (2011) and Marino et al. (2012).

SGB target stars were selected from the 3×3 mosaic of *HST* fields presented in Villanova et al. (2007) in order to cover the 5 SGBs of the $m_{\rm F435W}$,$m_{\rm F625W}$ CMD identified in that paper. In this paper we call the 5 SGBs as: A,B,C,D, and E (see Fig. 1).

Stars were selected for the observations in order to have no neighbors closer than 0.6 arcsec and brighter than $m_{\rm F625W}$+2.5 mag, where $m_{\rm F625W}$ is the magnitude of the target, to avoid possible contamination. Target stars were then further cleaned for any remaining contamination during the data analysis process as explained in the following section. We identified our targets also in the ground-based photometry by Bellini et al. (2009). This was done to obtain V magnitudes, needed to estimate gravity (see next section). However, in a few cases we found that the V ground based magnitude was widely discrepant compared to $m_{\rm F625W}$, probably because of the crowding. In order to remove this problem we decided to used an *interpolated* V magnitude (V_i). To do that we plotted V vs $m_{\rm F625W}$. The relation is linear, so we fitted a straight line using a 3σ clipping rejection algorithm. Finally we adopted V_i obtained from this relation and the appropriate $m_{\rm F625W}$ magnitude of each star.

The data were reduced using GIRAFFE pipeline 1.13 (Blecha et al. 2000), which corrects the spectra for bias and flat-field. (See http://girbldrs.sourceforge.net/ for documentation on the GIRAFFE pipeline and software.). A sky correction was applied to each stellar spectrum by subtracting the average of ten sky spectra that were observed simultaneously with the stars (same FLAMES plate). The wavelength calibration uses calibration-lamp spectra taken the following day with respect to the observations. Finally, each spectrum was normalized to the continuum. The resulting spectra have a dispersion of 0.05 Å/pixel and a typical S/N ∼25-40, with a median value of 35.

We used the fxcor utility of IRAF to measure the radial velocity, which we then converted to heliocentric. The error in radial velocity is typically about ∼1 km/s. Considering the mean radial velocity of ω Cen (∼232 km/s, Reijns et al. 2006), the velocity dispersion in the inner part of the cluster (∼15 km/s, Reijns et al. 2006), and the observational errors, all of the stars with radial velocity in the range 180-300 km/s were considered members.

The coordinates, magnitudes, and radial velocities of our members are reported in Tab 3. This table reports on the final targets after eliminating binaries and contaminated objects, as explained in the following section.

3. Abundance measurements

First of all we checked for any possible residual contamination of our targets by neighbor stars that can be easily identified in our photometry. To be conservative and avoid any misinterpretation of the data, we finally decided to retain only those targets with no contamination, i.e. those targets with no neighbors brighter than $m_{\rm F625W}$+2.5 mag within 3 times the FWHM of our observations. This guarantees us that the final metallicity is not altered by contamination effects. We had to reject 264 stars.

Second, we checked for possible binaries looking for radial velocity variations. We expect most binaries to be composed of a SGB and a MS; such systems should be brighter on average with respect to the single star sequence. For this reason they would appear younger than they really are. For each target we have 4/5 radial velocities obtained in different epochs, with an epoch range of a few weeks. So we obtained the r.m.s. for each star and finally the r.m.s. distribution (not reported here). According to this distribution we flagged as binaries all those stars that show a r.m.s. larger than 7 km/s. We rejected 14 stars as binaries.

After the contamination and the binary checks, we were left with 172 objects that are plotted in Fig. 1.

As in Villanova et al. (2007), we derived effective temperatures ($T_{\rm eff}$) from the $m_{\rm F435W}$ − $m_{\rm F625W}$ color in the *HST* CMD. The relation between color and $T_{\rm eff}$, as a function of [M/H] (by which we mean the global metallic-

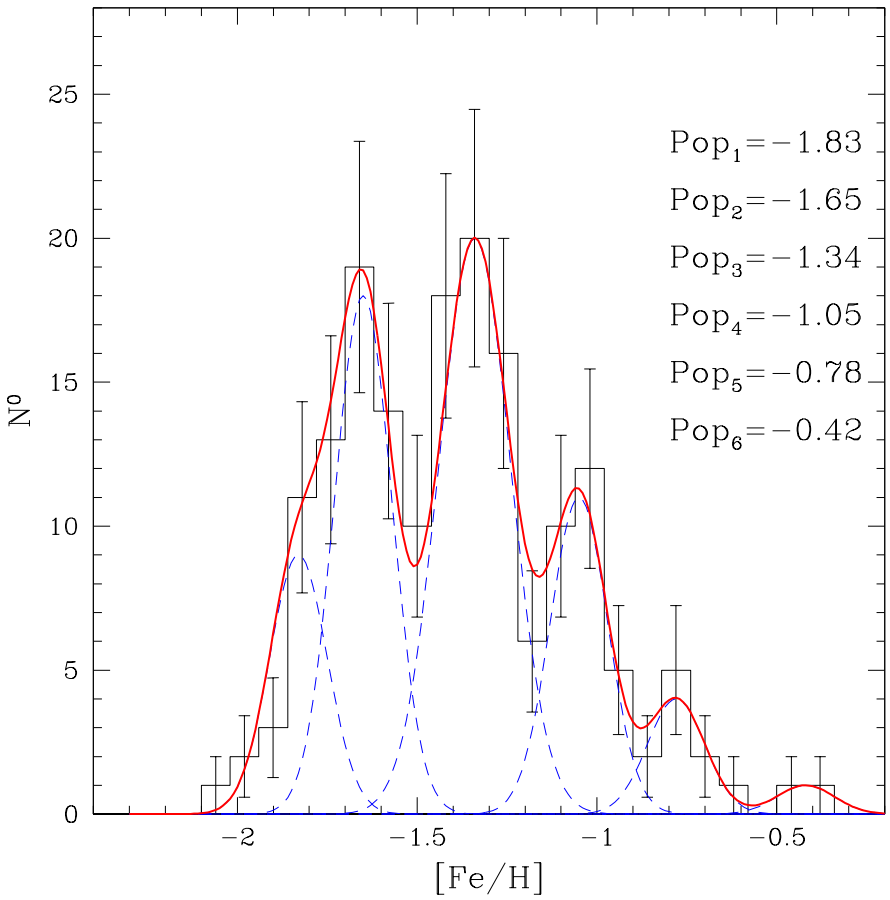

Fig. 3.— [Fe/H] distribution of our entire sample. Each sub-population is represented by a blue Gaussian (dashed line) and its mean metallicity is indicated. The continuous red line is the sum of the Gaussians fitting the observational data.

ity, including alpha elements), was derived from isochrones by Pietrinferni et al. (2006)[2]. Colors were de-reddened using the absorption coefficients listed in Table 3 of Bedin et al. (2005), adopting $E(B-V) = 0.115$. As a first guess for the [M/H] to be used in the color-[M/H]-temperature relation, we adopted [Fe/H] = −1.5, the mean metallicity of ω Cen stars, along with an α-enhancement of 0.4 dex for all stars (see Johnson & Pilachowski 2010). The [M/H] was derived from the adopted [Fe/H] and the alpha enhancement from the prescription by Salaris et al. (1993), along with the corresponding $T_{\rm eff}$ from the color-[M/H]-temperature relation. Using this value for $T_{\rm eff}$, we calculated $\log g$ and $v_{\rm t}$ and measured a new [Fe/H] abundance as described below. Then for each star the values of $T_{\rm eff}$ and [Fe/H] were changed in an iterative process, till convergence (when $\log g$ and $v_{\rm t}$ change less than 0.02 dex and 0.02 km/s respectively).

As noted by Villanova et al. (2007), the effect of variations in helium content on the relation between color and temperature is of the order of ∼10 K in temperature for SGB stars, which translates into a change of ∼0.01 dex in metallicity. Such small changes can be neglected.

[2]http://basti.oa-teramo.inaf.it/index.html

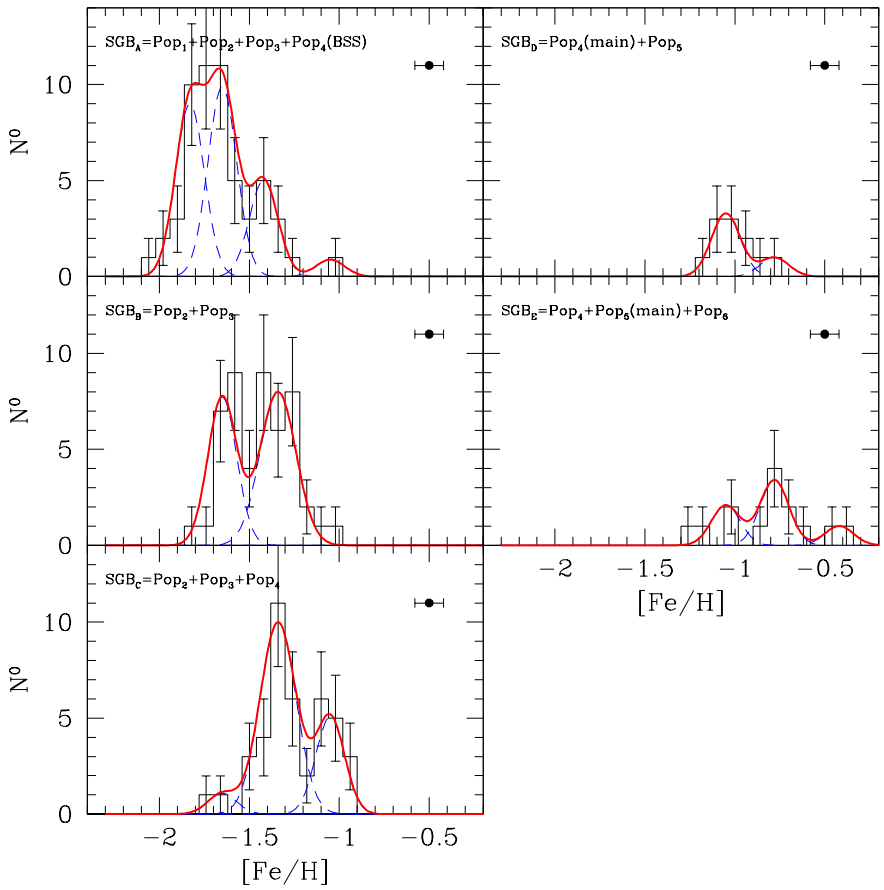

Fig. 4.— [Fe/H] distribution of each SGB. Each sub-population is represented by a blue Gaussian (dashed line). The continuous red line is the sum of the Gaussians fitting the observational data. For each SGB we indicated the populations that we could fit. Errorbars in the top-right part of each panel represent the observational error on the [Fe/H] measurement.

The gravity $\log g$ was calculated from the elementary formula

$$\log\left(\frac{g}{g_\odot}\right) = \log\left(\frac{M}{M_\odot}\right) + 4\log\left(\frac{T_{\rm eff}}{T_\odot}\right) - \log\left(\frac{L}{L_\odot}\right).$$

The mass $M/M_\odot$ was derived from isochrone fitting. The luminosity $L/L_\odot$ was derived from V_i, assuming the absolute distance modulus $(m-M)_0 = 13.75$ found by Van de Ven et al. (2006), and the reddening adopted above. The bolometric correction (BC) was derived from the BC-$T_{\rm eff}$ relation of Alonso et al. (1999). Finally, the microturbulence velocity came from the relation (Gratton et al. 1996):

$$v_{\rm t} = 2.22 - 0.322\log g.$$

The adopted atmospheric $T_{\rm eff}$, $\log g$, and v_t are listed in Tab 3.

The metal content was obtained by comparison with synthetic spectra calculated using MOOG (Sneden 1973). The model atmospheres of Kurucz (1992), used throughout this paper, assume $N_{\rm He}/N_{\rm H} = 0.1$, corresponding to $Y = 0.28$ by mass. The bMS and the related SGB stars (i.e., stars with the same metallicity as the bMS stars), are thought to have a helium content $Y \sim 0.38$ As

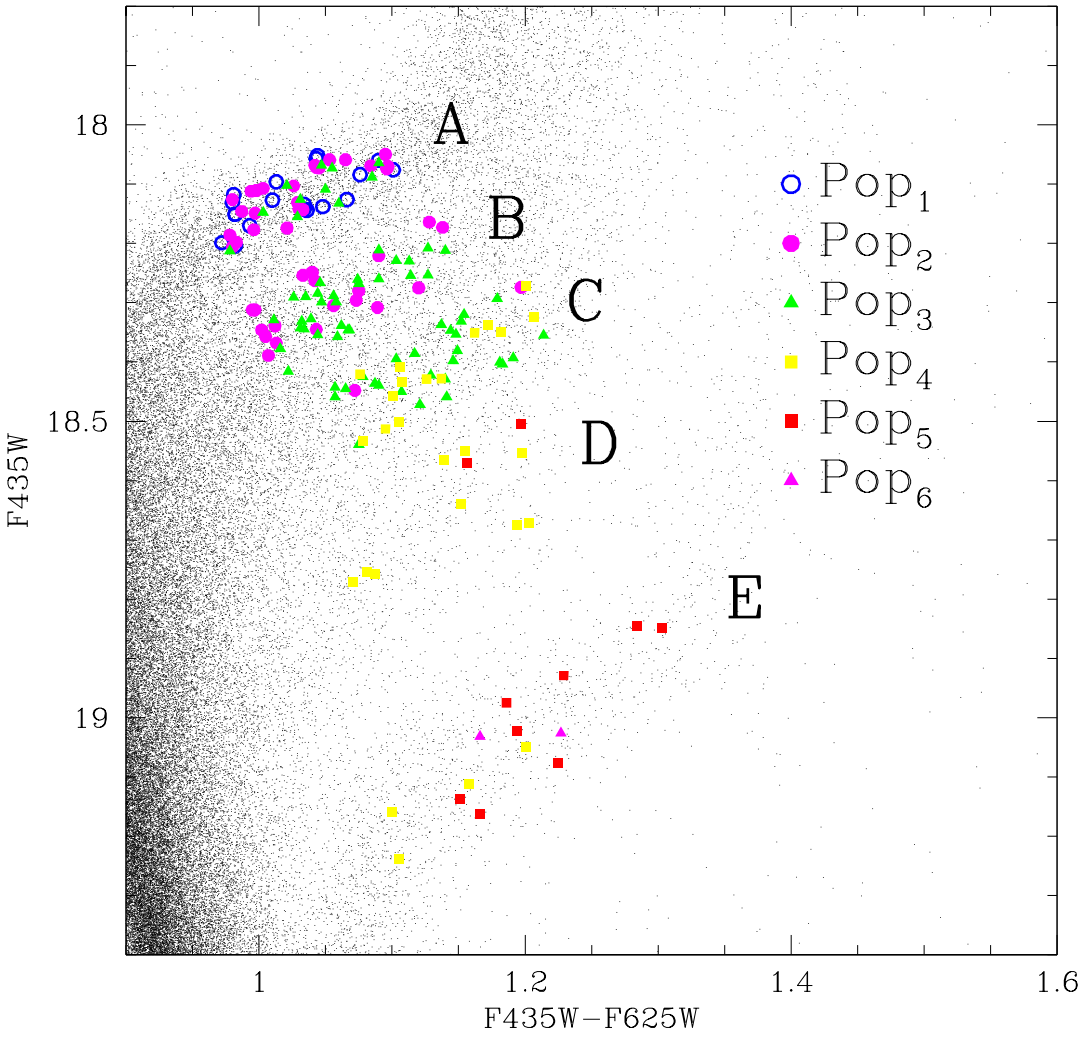

Fig. 5.— Position on the CMD of the subpopulations identified in this paper.

discussed in Piotto et al. (2005), the variation in the atmospheric structure due to this increase in helium introduces an systematic error smaller than 0.03 dex in the metal-abundance determinations, which is negligible.

Our [Fe/H] values were obtained from a comparison of each observed spectrum with five synthetic ones (see Fig. 2), calculated with different metal abundances. We used the regions at 6136-6138 Å and at 6191 Å for this purpose. These regions contain the only Fe lines not contaminated by telluric absorption and emission features and visible in all our spectra due to their S/N and to the T_{eff} and low metallicity of the targets. In the most metal-rich spectra other iron lines are visible, but to be homogeneous we had to choose those that are the only visible also in the most metal-poor targets. log(gf) of the lines were calibrated by spectrosynthesis on the Sun assuming logϵ(Fe)=7.50 and the solar spectrum by Kurucz et al. (1984).

The metallicity was obtained by minimizing the r.m.s. scatter of the differences between the observed and synthetic spectra. [Fe/H] values derived for our targets are listed in Tab 3.

At this point we must note the the [Fe/H] we obtained is based on the assumption of a standard $N_{\rm He}/N_{\rm H}$ content. However the cluster has a mean He content that varies from Y=0.25 for the most metal poor stars, to Y$\sim$0.39 for the most metal rich, according to Joo & Lee (2013). A larger He content implies a lower H content, and by consequence the real [Fe/H] value should be higher than that we obtained. For ΔY=0.14 we should apply a correction of Δ[Fe/H]=+0.09. However this would make the comparison with the literature difficult, so we prefer to use our present value and just warn the reader about this effect.

Because we have uncontaminated objects, the random internal error is dominated by the noise of the spectra. S/N ranges from 30 to 40 for most of the stars, while the faintest have S/N$\sim$25 in the worst case. To estimate the error in [Fe/H] we used Monte Carlo simulations. For this purpose we calculated a spectrum representative of the two most populous and extreme populations, the brightest at [Fe/H]$\sim$-1.8, and the faintest at [Fe/H]$\sim$-0.8. Then we added noise to each one in order to obtain 1000 new spectra that simulate the real ones. Finally we measured the [Fe/H] of each simulated spectrum. Both for brighter and fainter targets we found σ([Fe/H])=0.08 dex. This is probably because the decrease of S/N is compensated by the increase of the mean metallicity, which gives stronger spectral lines. Another way to estimate this error is to use the formula by Cayrel (1988):

$$\sigma_{\rm EQW} \sim 1.06 \times \sqrt(FWHM \cdot \delta x)/(S/N)$$

In our case FWHM=0.35 Åand δx=0.05 Å. For the median S/N of our spectra ($\sim$35), the expected $\sigma_{\rm EQW}$ is 4 mÅ. This translates into σ([Fe/H])=0.07 if we consider that we used three iron lines to estimate abundances, which is close to the value we obtained with the Monte Carlo simulations.

To this error we should add (in quadrature) the error due to photometric uncertainty in the colors; the error in color is typically of the order of 0.01 magnitude, which translates into a 0.02 dex error in abundance (see Villanova et al. 2007). Finally we adopt an overall uncertainty of 0.08 dex for [Fe/H]. This is the internal random error in our metallicity measurement. In addition there can be a systematic error of the order of 0.15–0.20 dex, because of systematic uncertainties in the effective temperature scale, in the model atmospheres, in the distance and reddening. The systematic errors do not affect the relative metallicities of the different stellar populations of ω Cen that we will discuss in later sections.

4. Results

First of all we plot the iron distribution of the entire sample in Figure 3. Then in the following plot (Fig. 4) we report the iron distribution of the five SGB branches of figure 1 separately.

The first basic thing we note is that according to our analysis any of the SGBs has a distribution in metallicity with a spread that exceeds the observational errors. Such an error is plotted in Fig. 4 as an errorbar in the top-right part of each panel. In addition each SGB displays several peaks, that allowed us to identify a certain number of subpopulations that form the cluster.

The identification of the metallicity-based subpopulations was done in order to reproduce at the same time the metallicity distribution of the entire sample and the metallicity distribution of the single SGBs. We could identify 6 of them termed:

$$Pop_1 : [Fe/H] = -1.83$$
$$Pop_2 : [Fe/H] = -1.65$$
$$Pop_3 : [Fe/H] = -1.34$$
$$Pop_4 : [Fe/H] = -1.05$$
$$Pop_5 : [Fe/H] = -0.78$$
$$Pop_6 : [Fe/H] = -0.42$$

Their presence and their mean [Fe/H] value are justified by the following analysis.

In the figures each subpopulation was fitted with a Gaussian (blue dashed line) having a σ that was allowed to vary up to $\pm$0.02 dex around our theoretical uncertainty of 0.08 dex in order to obtain a better fit. In each figure the continuous red

line is the sum of all the single Gaussians. We allowed also the mean [Fe/H] value of each subpopulation to vary of few hundredth of dex in order to obtain the best match possible with the data.

Fig. 4 shows that SGB_A is dominated by Pop_1 and Pop_2, but Pop_3 is clearly visible. In addition there is a faint peak that could correspond to Pop_4. The most probable explanation is that this peak corresponds to evolved blue straggler stars (BSS).

SGB_B is composed of a mix of Pop_2 and Pop_3.

In SGB_C Pop_3 and Pop_4 are clearly visible as two well defined peaks. The histogram shows also a tail with a secondary peak at [Fe/H]$\sim$-1.7. We interpret this as Pop_2.

SGB_D is dominated by Pop_4, but there is a tail that corresponds to Pop_5.

SGB_E is dominated by Pop_5, but Pop_4 is clearly visible as a well defined tail, while Pop_6, in spite of being formed by only 2 stars, forms a separated peak.

If we consider Fig. 3, we can clearly identify Pop_2, Pop_3, Pop_4, Pop_5, and Pop_6 as well defined peaks. Pop_1 forms a low metallicity tail and not a peak, but if we remove it we cannot fit properly the iron distribution.

5. Comparison with the literature

We already presented in the introduction the most recent papers that discuss the number and iron content of the sub-populations of ω Cen. In this section we discuss how those results can be interpreted in the light of what we have found here. We underline the fact that, due to the very extensive literature and to the very different methodologies used to study this cluster, we focus our attention only on those papers that try to identify the number of sub-populations based on their [Fe/H] content.

Sollima et al. (2005) found 4 stellar populations at [Fe/H]=-1.7,-1.3,-1.0, and -0.6. Looking at their figure 4, we can suggest that their population at -1.7 is a mixture of Pop_1, and Pop_2, that at -1.3 is our Pop_3, that at -1.00 is our Pop_4 and that at -0.6 is our Pop_5.

Villanova et al. (2007) found 3 stellar populations at [Fe/H]=-1.68,-1.37, and -1.14. Looking at their figure 15, the population at -1.68 can be identified as a mixture of Pop_1 and Pop_2, while that at -1.37 is our Pop_3. The group at -1.14 is our Pop_4.

Calamida et al. (2009) found 6 peaks in the iron distribution at [Fe/H]=-1.73,-1.29,-1.05,-0.80,-0.42, and -0.07 dex. Looking at their figure 17, the group at -1.73 can be identified as a mixture of Pop_1, and Pop_2. In particular Pop_1 is visible as a peak at [Fe/H]$\sim$-1.8$\div$-1.9, not pointed out by the authors. The peak at -1.29 is our Pop_3, while the peak at -1.05 is our Pop_4. Their peaks at -0.80 and -0.42 are our Pop_5 and Pop_6 respectively. In particular the identification of the same population at [Fe/H]=-0.42 in two independent datasets make us confident that Pop_6 is real. On the other hand we do not have any trace of their peak at -0.07. An explanation could be that the corresponding population forms a weak SGB branch fainter than SGB_E, so we did not recognize it in our CMD, and we did not point any fiber on its stars, or that it is too centrally concentrated, so we missed it in the fiber pointing

Johnson & Pilachowski (2010) identified four groups at [Fe/H]=-1.75,-1.50,-1.10,-0.75. Looking at their figure 8, the populations at -1.75, -1.10, and -0.75 can be identified with our Pop_1+Pop_2, Pop_4, and Pop_5 respectively. Their peak at -1.50 does not correspond to any of our populations.

We do not confirm the presence of a very metal poor population ([Fe/H]$\sim$-1.9), as suggested by Pancino et al. (2011). However our data do not have the required accuracy and statistics to identify such a feature.

Finally we compare our results with Marino et al. (2011). These data show clear peaks at [Fe/H]=-1.76, -1.60,-1.00, and -0.76 that correspond to our Pop_1,Pop_2,Pop_4, and Pop_5 respectively. Pop_3 is visible as a tail of Pop_2.

6. The age spread and the age-metallicity relation

After having determined the sub-populations that form the cluster and their distribution on the SGB, we can discuss the implication of the present results on the age spread that, according to Villanova et al. (2007), affects the cluster and that should be of the order of several Gyrs. This is a controversial topic, because some authors suggest that ω Cen does not have any age spread at

Table 1
Most probable [Fe/H] range, SGB correspondence, and age-spread for each sub-population.

Population	[Fe/H]	SGB	Age-spread (Gyrs)
Pop_1	-1.83	A	0
Pop_2	-1.65	A+B(+C)	2(4)
Pop_3	-1.34	A+B+C	4
Pop_4	-1.05	C+D+E	7
Pop_5	-0.78	E(+D)	0(4)
Pop_6	-0.42	E	0

all (e.g. Sollima et al. 2005).

We start by estimating the range in magnitude each sub-population covers at the level of the SGB. We do not consider peaks identified as BSS.

In order to visualize the spread in magnitude of each population, we plot in Fig. 5 their position on the SGB. The membership of each star was decided based on which Gaussian dominates at its metallicity in Fig. 4. The [Fe/H] interval assigned to each population changes from one SGB branch to the other in order to minimize the contamination due to measurement errors. Of course some contamination remains, but with the given error in metallicity it is impossible to separate completely the six groups of stars. For the following discussion we assume the each population has no intrinsic [Fe/H] spread, and that the enlargement associated to each peak in the [Fe/H] distribution histograms is totally due to the measurement error. This is justified by the fact that Gaussians with a σ of 0.08 dex (that is our internal measurement error) well fit the total [Fe/H] distribution of Fig. 3.

Pop_1 forms only SGB_A. Pop_2 forms part of SGB_A, SGB_B, and maybe SGB_C, so its spread is of the order of 0.2÷0.4 mag. Pop_3 forms part of SGB_A, SGB_B, and SGB_C so its spread is of the order of 0.4 mag. Pop_4 forms SGB_C, SGB_D and SGB_E so its spread is of the order of 0.7 mag. Pop_5 forms SGB_E and maybe SGB_D so its spread is < 0.4 mag. Pop_6 does not show any spread and all its stars belong to SGB_E.

The correspondence between populations and the five SGBs is given in Tab. 1.

Before giving an estimation of the age spread of each population we must address some further considerations.

The first concerns the interval in age that corresponds to a $\Delta m_{\rm F435W}$ of 0.1 mag on the SGB. In Villanova et al. (2007) we already performed this exercise, and it turns out that the exact value depends both on metallicity and helium content. However a good aproximation is $\sim$1 Gyr per 0.1 mag.

The second concerns the total CNO content of each population. NGC1851 has a double SGB (Milone et al. 2008), where the two population are separated of about 0.1 mag in luminosity. This implies an age difference of about 1 Gyr if the two populations have the same CNO. However, Cassisi et al. (2008) showed that a CNO difference of 0.3 dex can reduce the age difference to 100 Myrs.

To investigate this point we plotted in Fig. 6 the total CNO content as a function of the metallicity ([Fe/H]) using data from Marino et al. (2012, crosses), D'Orazi et al. (2011, open circles), and Villanova et al. (2014, in preparation, filled points). Marino et al. (2012) and Villanova et al. (2014) well sample the region below [Fe/H]=-1.0, while D'Orazi et al. (2011) and Villanova et al. (2014) are used to sample the more metal rich part above [Fe/H]=-1.0. We draw the mean trend that is represented by the black continuous line, while the black dashed lines are the mean trend shifted vertically by $\pm$0.08 dex, that is the mean r.m.s. of the data (see below). We notice that the mean CNO content has two different linear trends. the first, from [Fe/H]$\sim$-2.0 to [Fe/H]$\sim$-1.5 has a

slope of ∼0.76, while the other from [Fe/H]∼-1.5 to [Fe/H]∼-0.5 is flatter with a slope of ∼0.12. After that we calculate the spread of the points around the mean trend, and found that the dispersion of [CNO/Fe] is σ=0.08 dex. This is a small value, comparable with the typical measurement error of any chemical abundance determination procedure (e.g. Villanova et al. 2011). So we can assume that any intrinsic spread in CNO (at a given metallicity), if present at all, is negligible. A more straightforward procedure would be the direct calculation of the measurement error on the [C+N+O/Fe] quantity, that depend on the error on temperature, gravity, metallicity, microturbulence, and on the S/N, but this is out of the aim of this paper. Our conclusion is that we can assume a constant CNO content within each sub-population.

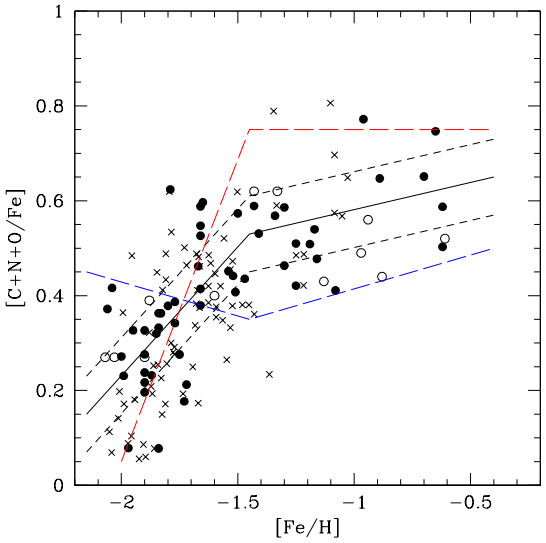

Fig. 6.— Mean trend of [C+N+O/Fe] vs. [Fe/H] for stars in ω Centauri. See text for more details.

We can now translate the magnitude spread into an age spread. Results are reported in Tab. 1. Three populations (Pop_2, Pop_3, and Pop_4) have an age-spread of at least 2 Gyrs. Pop_4 shows a surprisingly large age-spread.

Pop_1 and Pop_6 do not show an age-spread. On the other hand Pop_5 possibly occupies also SGB_D, but the number of its possible stars is so small (a total of 2) that we prefer to live the question open and assign it an age-spread of 0, and to put the possible membership to SGB_D and the correspondent age-spread within parenthesis in Tab. 1. Also Pop_2 suffers the same problem and its membership to SGB_C is uncertain. So we decided again to put it within parenthesis in Tab. 1, together with the relative age-spread.

So we conclude that ω Centauri shows clear evidence of a significant age-spread, at least for three of its populations, when they are identified based on metallicities alone.

The next step is to transform all the information we have, i.e. the metallicity and magnitude of each star, in an age-metallicity relation, taking advantage of the fact that the SGB is the place in the CMD most sensitive to age effects. The aim is to transform the F435W magnitude of each star into an age. However there are several effects that can be taken into account using isochrones (Pietrinferni et al. 2006). The most obvious one is the fact that stars of the same age but different metallicity have different F435W magnitude, with the most metal rich being also the faintest. We found that a difference of 1.0 dex in metallicity corresponds to a F435W difference of 0.64 mag on average, taking the other parameters constant. On the other hand the α-enhancement is not an issue because all stars have the same α content at all metallicities (Johnson & Pilachowski 2010, Fig. 13). A further effect to take into account is the He content. In Piotto et al. (2005) we showed that stars with [Fe/H]∼-1.7 have a normal He content (Y∼0.25), while stars with [Fe/H]∼-1.4 are He-enhanced (Y∼0.38). Recently Joo & Lee (2013) published a more detailed He trend that we adopted here. According to this trend, all stars with [Fe/H]<-1.55 have Y=0.25, all stars with [Fe/H]>-1.31 have Y=0.39, while for stars in between Y linearly increases from [Fe/H]∼-1.55 to [Fe/H]∼-1.31. Again, using isochrones with different He content, we found that ΔY=+0.1 corresponds to an increase of F435W of ∼0.05 mag, taking the other parameters constant. We notice that the large uncertainty on the He-[Fe/H] relation is compensated by the small effect of Y on the F435W magnitude (much lower than that due to the metallicity). The CNO trend was already discussed above. We just take it into account using the relation published by Marino et al. (2012, section 5) that is valid for [Fe/H]<-1. In this iron regime the effect of CNO enhancement is indepen-

dent of metallicity. For [Fe/H]$\sim$-0.4 (the upper limits of our metallicity range) isochrones show that the effect of CNO enhancement on age is 3 times larger than for the [Fe/H]<-1 regime, taking the other parameters constant. We linearly interpolated in between.

Finally, as already said, for a given metallicity, He content, and C+N+O content, a 0.1 mag. difference in F435W corresponds to an age difference of $\sim$1 Gyr, taking the other parameters constant. We verified also that all the quantities we assumed to transform F435W into age apart from the CNO content (i.e. 0.64 mag/dex for the metallicity, 0.05 mag for a change of 0.1 in Y) are fairly constant over the entire interval of ages and metallicities covered by our stars. They are reported in Tab. 2 for reference.

In order to take into account also the SGB tilt (see Fig. 1), we proceeded as in Villanova et al. (2007), i.e. we fitted a straight line to the upper SGB, and calculated the distance of each star with respect to this line. We notice that the five SGBs of Fig. 1 are not perfectly parallel to each other, but this does not affect our final result in a significant way. All the quantities discussed before (i.e. 0.64 mag/dex, 0.05 mag for a change of 0.1 in Y, and 0.1 mag/Gyr) are related to a vertical difference of the magnitude F435W in the CMD, and for this reason they were transformed to this new reference system parallel to the upper SGB too.

Error on the final age is a function of the [Fe/H] difference between two stars. For targets of the same metallicity and, as a consequence, of the same He and CNO content, it is dominated by the error on the magnitude and [Fe/H] value. To estimate the error in this case we used a Monte Carlo simulation. We took an artificial star representative of the entire sample assigning it a metallicity of [Fe/H]=-1.50 a magnitude $m_{\rm F435W}$=18.5 and a color $m_{\rm F435W} - m_{\rm F625W}$=1.12. After that we generated 10.000 stars according to a random Gaussian distribution centered on these values and with a dispersion σ on $m_{\rm F435W}$ and $m_{\rm F625W}$ of 0.01 mag (the typical photometric error for a SGB star), and on the metallicity of 0.08 dex. Finally we estimated the age of these 10.000 stars using the same method described above for the real stars. The result is the errors reported in Fig. 7 as contours. The inner contour is the 1σ error, the contour in the middle is the 2σ error, while the outer contour is the 3σ error.

For completeness we should add the random error due to some possible He spread for a given Fe abundance that overlaps the He-Fe relation obtained by Joo & Lee (2013). Let's take an hypothetic star in the middle of the He range we assumed, i.e. a star with Y=0.32, and consequently [Fe/H]=-1.43. A difference in its He abundance from the adopted value would not influence its age directly because the dependence of age on He is very weak, but would affect its age determination through its [Fe/H] value. In fact a larger He content implies a lower H content, and by consequence the real [Fe/H] value should be higher than that we would have obtained using the method of section 3. A reasonable assumption is that our hypothetical star can have an He value in the range of ΔY=$\pm$0.07 around Y=0.32. This is half of the total He interval obtained by Joo & Lee (2013, ΔY=0.14). A fast calculation shows that this corresponds to a [Fe/H] correction of $\pm$0.045 dex. This is negligible compared to our error on [Fe/H] of 0.08 dex. It is also an overestimation because we should use not ΔY=$\pm$0.07 for our purposes, but the σ of the He spread that, if the He distribution is a Gaussian, is of about 0.14/6$\sim$0.02. This makes the impact of any possible He spread for a given metallicity totally negligible compared with the error shown in Fig. 7.

For stars at the extremes of the [Fe/H] interval, uncertainties in the He and CNO trends also must be considered. instead. While the impact of the He trend uncertainty is negligible, the impact of the CNO trend uncertainty will be discussed in the next subsection.

We underline the fact that the ages obtained so far are relative ages, and errors we estimated are errors on relative ages. Absolute ages were obtained applying a rigid shift to the whole sample in order that the oldest stars have the age of the Universe. Systematic error on absolute ages is surely larger than 1 Gyr, but for our purposes it is not a concern.

The final product of this procedure is the age-metallicity relation presented in Fig. 7. Ages derived for our targets are listed in Tab 3. Our data (black points) appear to follow five well defined strips. This is not a real effect but a consequence of our target selection that was focused on the five

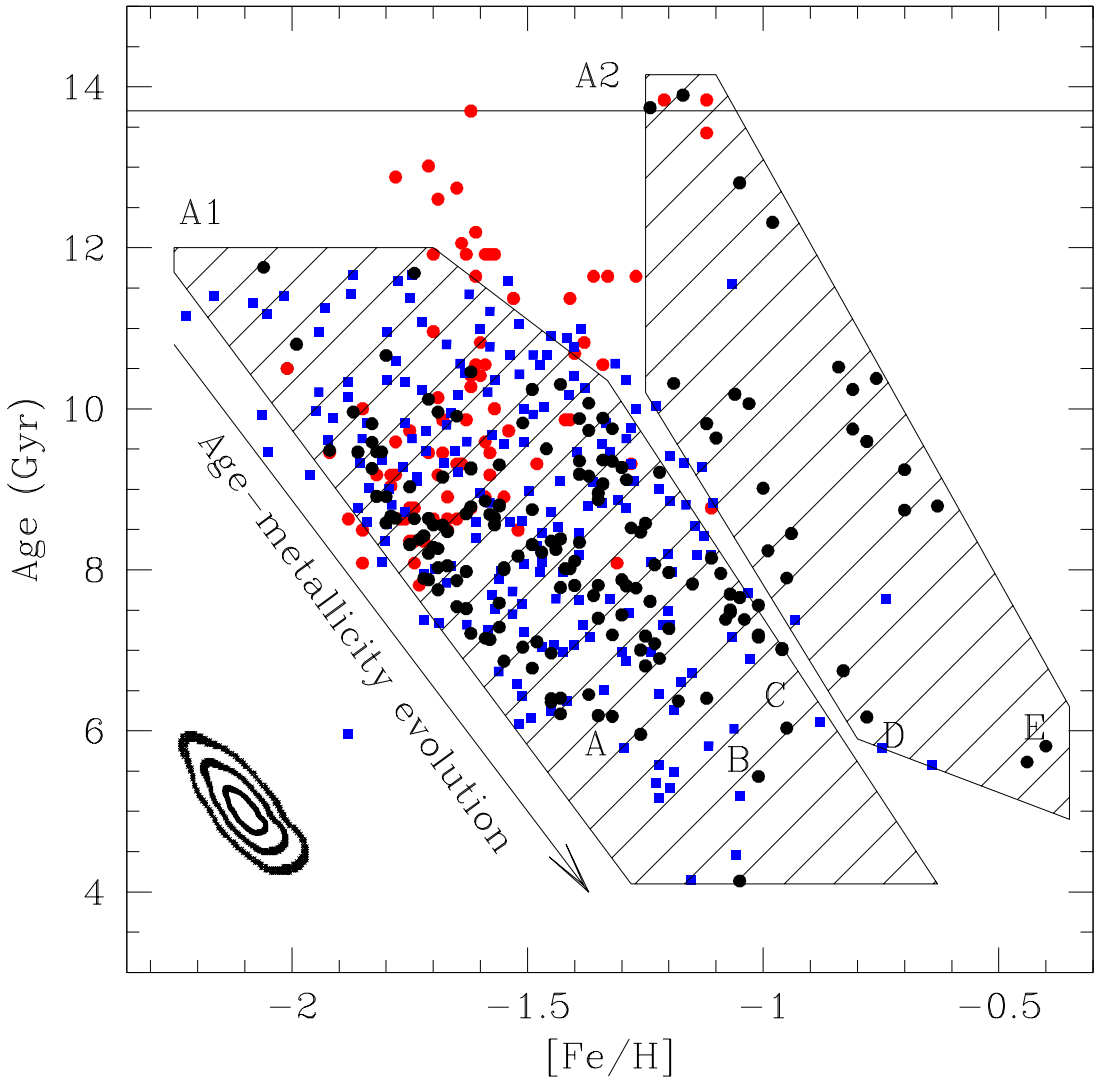

Fig. 7.— The age-metallicity relation for ω Centauri. Contours represents the 1σ, 2σ, and 3σ errors respectively. Red points are data from Villanova et al. (2007), while blue points are data from Hilker et al. (2004). See text for more details.

SGBs. The correspondence between the five SGBs and the five strips is indicated by the five letters that identify the SGBs in Fig. 1. Red points are the age-metallicity relation by Villanova et al. (2007). We apply a vertical shift to our points in order to match the age of the three old metal rich stars ([Fe/H]$\sim$-1.15, age$\sim$13.7 Gyrs). We note that red points in the -1.8<[Fe/H]<1.3 regime are older than black points. This is because in Villanova et al. (2007) we did not take into account the affect of the C+N+O content.

Blue points are the age-metallicity relation by Hilker et al. (2004). Again, we shifted vertically these data in order to match the black points.

The easiest way to interpret Fig. 7 is to divide our points in two shaded areas, one that follows the trend shown by metal poor stars (A1), and

TABLE 2

THE SENSITIVITY OF F435W MAGNITUDE ON METALLICITY, Y,AND AGE (FIRST THREE RAWS), AND THE SENSITIVITY OF AGE ON CNO CONTENT (LAST TWO RAWS).

Parameter	Variation	F435W/Age variation
Δ[Fe/H]	$\pm$1.0 dex	$\pm$0.64 mag
ΔY	+0.10	$\pm$0.05 mag
ΔAge	$\pm$1.0 Gyr	$\pm$0.10 mag
ΔCNO([Fe/H]$\leq$-1.0)	$\pm$1.0 dex	$\mp$3.3 Gyr
ΔCNO([Fe/H]=-0.4)	$\pm$1.0 dex	$\mp$9.9 Gyr

the other that follows the trend shown by metal rich stars (A2). Although the A2 group is less populated than A1, its presence is definitively proven by our results, which is one of the most surprising results of this paper. In both cases the progenitors of each relation appear to be a quite old group of stars, that for A1 have [Fe/H]$\sim$-2.0 and age$\sim$11.0 Gyrs, while that for A2 have [Fe/H]$\sim$-1.2 and an age of almost 14 Gyrs. Because of their ages and metallicity differences, it is very difficult that the second derives from the first by some kind of chemical evolution, so they should be assumed as two independent primordial objects. Then in each area stars appear to evolve toward higher metallicities following the arrow labeled with *age-metallicity evolution*. We underline the fact that the age-metallicity evolution we draw is only a first intent of interpretation. Future works could change the scenario we are proposing significantly.

The age-metallicity relation within A1 was already presented in Hilker et al. (2004) as shown by the blue squares. That within A2 is evidenced here for the first time due to our much more complete SGB sample. The presence of two age-metallicity relations can easily explain the age spread of Pop_4, that appears to be very large. It simply comes from the superposition of the two age-metallicity relations in the range -1.20<[Fe/H]<-0.90.

The fact that the oldest population is more metal-rich compared with the bulk of the metal-poor stars in a globular cluster like object is something that goes against common sense. One would have expected a monotonically decreasing age-metallicity relation, or at least that the most metal-poor and metal-rich stars were coeval, if the initial chemical enrichment would have occured in a short time-scale (<1 Gyr). The only way to rejuvenate A2 stars and place it on the top of A1 is to assume a total CNO $\sim$1.8 dex larger then its actual value, i.e. all star belonging to the A2 group should have [C+N+O/Fe]$\sim$2.3 dex, that is a much higher value than anyone observed not only in ω Cen, but in any Galactic object. Only some very metal-poor stars (Sivarani et al. 2006) show extremely enhanced C, N, and O (with [N/Fe] up to $\sim$+3.0), but in this case this is attributed to contamination by an AGB or massive fast-rotating companion.

To complete our interpretation, it is remarkable that each relation has an age difference (difference between the youngest and oldest star, including also the errors) of $\sim$3 Gyrs for a given [Fe/H] value.

At this point it is natural to propose that ω Centauri is the result of the merging of two independent objects (dwarf galaxies?) or of two independent parts of a single larger object, the first having the the oldest stars more metal poor ([Fe/H]$\sim$-2.0), the second having the oldest stars more metal rich ([Fe/H]$\sim$-1.2). Each object or part had its own independent evolution in the age-metallicity plane, at least down to 10 Gyrs. The evolution ended at $\sim$6 Gyrs for both of them. If they merged before or after the full evolution of the stars in the age-metallicity plane, and if and how they interacted, is very hard to say.

6.1. The impact of the uncertainty of the [C+N+O/Fe] vs. [Fe/H] relation on the age-metallicity relation

As discussed in Marino et al. (2012), the total CNO content can heavily influence the final age of a star and, in our case, the age-metallicity relation. For this reason we performed the following test in order the check how a incorrect estimation of the [C+N+O/Fe] trend as a function of [Fe/H] presented in Fig. 6 can alter the final result. We firstly estimated the two most extreme fits of the data, the first with the highest [C+N+O/Fe] value at [Fe/H]$\sim$-2.0 and the lowest for [Fe/H]>-1.5. This is plotted as a blue dashed line in Fig. 6. The second with the the lowest [C+N+O/Fe] value at [Fe/H]$\sim$-2.0 and the highest for [Fe/H]>-1.5. This is plotted as a red dashed line in Fig. 6. We underline that those fits are completely unreliable, but we want to check if also in the worst case our conclusions about the age-metallicity relation are supported. We report the result of this test in Fig. 8. The panel on the left was obtained with the blue fit, while the one on the right with the red fit.

We see that the presence of the two independent relations A1 and A2 is confirmed. In the panel on the left the oldest stars in A1 are as old as the oldest stars in A2, while in the one on the right, oldest stars in A1 are $\sim$4 Gyrs younger. This test confirms our hypothesis of the presence of two old, unrelated population in ω Centauri with very different iron contents. On the other hand, each relation shows an age difference of 4 Gyrs (in the first case) or 3 Gyrs (in the second case) for a given [Fe/H] value.

To check the impact of the uncertainty in CNO content on the age-spread for a given [Fe/H], we assume that the spread of 0.08 dex we estimated for [C+N+O/Fe] around the mean trend of Fig. 6 is totally intrinsic and not due to measurement errors. We lack any information about CNO for our stars, so we must proceed in a statistical way. In the previous section we showed that for a given metallicity the age difference is $\sim$3 Gyrs. A spread (σ) of 0.08 dex correspond to a maximum interval in the [C+N+O/Fe] value of $\sim$0.5 dex (i.e. $6\times\sigma$), that translates in an age interval of $\sim$1.5 Gyrs. If we subtract this value to the age difference we are left with 1.5 Gyrs. This means that the age difference is real and larger than 1.5 Gyrs (very likely $\sim$3 Gyrs because the spread of 0.08 dex in the CNO trend is almost totally due to measurement errors).

7. Conclusions

In this paper we analyzed 172 stars belonging to the SGB region of ω Centauri, in order to study the age and metallicity dispersion and the age-metallicity relation to have further clues of how this object was formed. For this purpose we obtained medium resolution spectra (R=22500) in the 6120–6405 Å range and measured the iron content of our stars using the same general approch as Villanova et al. (2007).

The accuracy of our measurements coupled with the age-sensitivity of the SGB, allowed us to find that any of the 5 SGBs of the cluster has a distribution in metallicity with a spread that exceeds the observational errors. In addition each SGB displays several peaks, that indicate the presence of several sub-populations. We could identify 6 of them based on their [Fe/H] value.

Taking advantage of the age-sensitivity of the SGB we showed that, first of all, at least half of the sub-population have an age spread of at least 2 Gyrs. These results are indeed very surprising, and we urge confirmation with additional data.

Then, considering all the possible contributors, we tranformed the magnitude of each star into a relative age, obtaining an age-metallicity relation. We underline the fact that we do not use absolute ages but values that consider only the differential SGB luminosity corrected for the differential He, [Fe/H], and CNO contents of each star. Because of this our final error on age is significantly reduced.

Our relation agrees well with those published previously, which however cover the age-metallicity space only partially.

The interpretation of the age-metallicity relation is not straightforward, but it is very likely that the cluster (or what we can call its progenitor) was initially composed of two old populations, but having different metallicities. The most metal poor had [Fe/H]$\sim$-2.0, while the most metal rich had [Fe/H]$\sim$-1.2, but the oldest stars in the metal-rich regime appear to be several Gyrs older than their oldest metal-poor counterparts. Because of their ages and metallicity, it is very difficult that

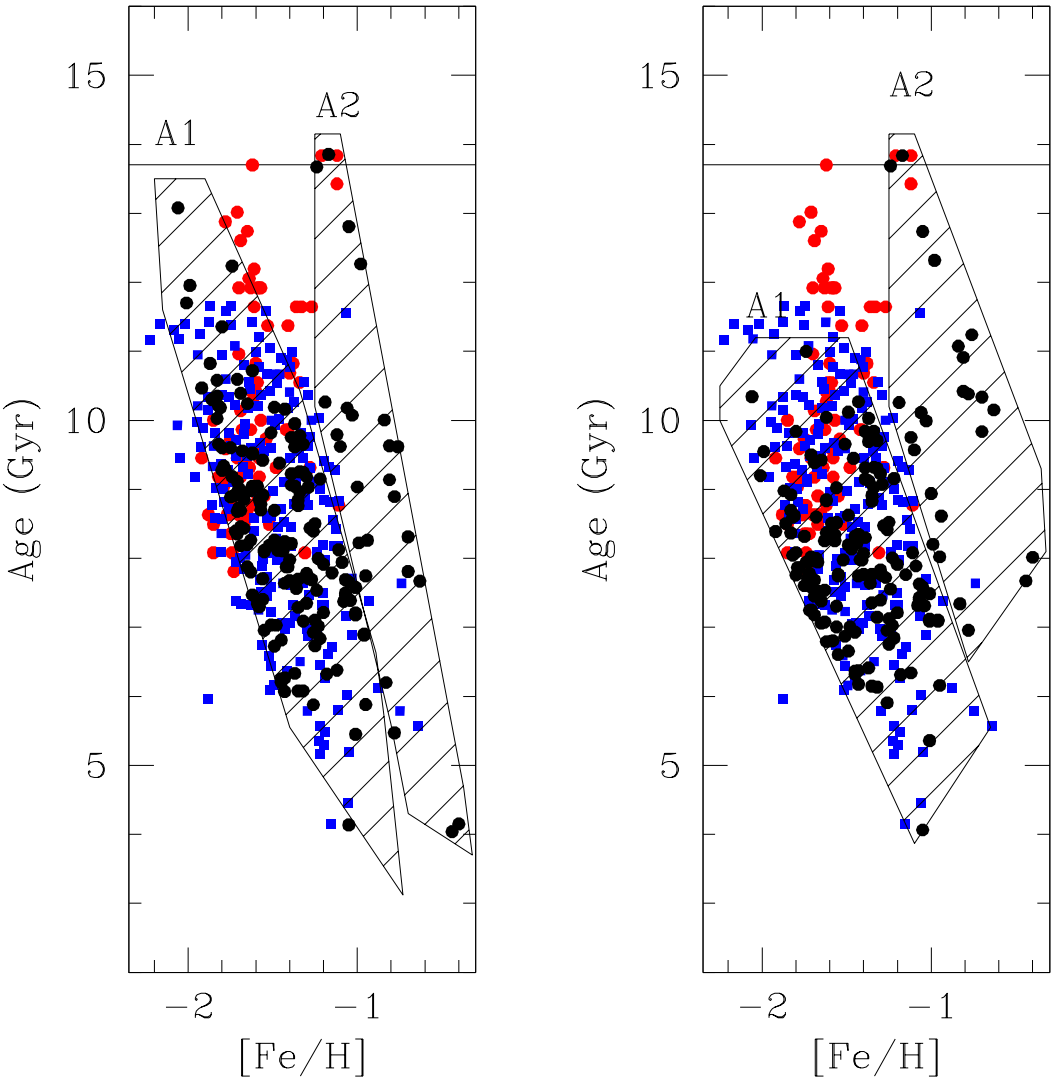

Fig. 8.— The impact of the uncertainty on the [C+N+O/Fe] vs. [Fe/H] relation on the age-metallicity relation. See text for more details

the second derives from the first by some kind of chemical evolution, so they should be assumed as two independent primordial objects. Afterwards, at first order, each one evolved chemically with iron that linearly increases with age according to our interpretation. This evolution stopped at ∼6 Gyrs. In any case they remain separated in the age-metallicity plane at least down to 10 Gyrs. In addition to this, each object shows an age spread of >2 Gyrs for a given metallicity. These conclusions are not altered by any possible uncertainty on the [C+N+O/Fe] vs. [Fe/H] relation.

These two primordial progenitors could correspond to two dwarf galaxies that at a given unknown time merged to form what is known today as ω Centauri. If they merged before of after the full evolution of the stars in the age-metallicity plane, and if and how they interacted, it is very hard to say. Clearly, much further work on this enigmatic object is required to help solve some of

its mysteries.

SV and DG gratefully acknowledge support from the Chilean BASAL Centro de Excelencia en Astrofisica y Tecnologias Afines (CATA) grant PFB-06/2007. S.V. gratefully acknowledges the support provided by FONDECYT N. 1130721. G.P., R.G.G., and S.C. acknowledge support by INAF under contract PRIN INAF 2009 Formation and Early Evolution of Massive Star Clusters. SC is grateful for financial support from PRIN-INAF 2011 *Multiple Populations in Globular Clusters: their role in the Galaxy assembly* (PI: E. Carretta), and from PRIN MIUR 2010-2011, project *The Chemical and Dynamical Evolution of the Milky Way and Local Group Galaxies*, prot. 2010LY5N2T (PI: F. Matteucci).

TABLE 3

PARAMETERS OF THE OBSERVED STARS. THIS TABLE IS PUBLISHED IN ITS ENTIRETY IN THE ELECTRONIC EDITION OF THE ASTROPHYSICAL JOURNAL. A PORTION IS SHOWN HERE FOR GUIDANCE REGARDING ITS FORM AND CONTENT.

ID	RA	Dec	$m_{\rm F435W}$	$m_{\rm F625W}$	T_{eff}	log(g)	v_t	[Fe/H]	RV	Age
	Degrees	Degrees	Mag.	Mag.	K	dex	km/s	dex	km/s	Gyr
SGB_A.1	201.60166667	-47.55916667	18.072	16.976	5592	3.69	0.99	-1.67	225.5	8.5
SGB_A.106	201.58141667	-47.44286111	18.107	17.104	5821	3.78	0.97	-1.62	221.9	7.2
SGB_A.107	201.60875000	-47.44119444	18.069	16.985	5611	3.69	0.99	-1.71	232.9	8.6
SGB_A.112	201.56883333	-47.43730556	18.112	17.118	5829	3.78	0.97	-1.71	232.8	7.9
SGB_A.12	201.59787500	-47.54488889	18.213	17.235	5909	3.85	0.95	-1.49	229.6	6.8
SGB_A.127	201.76162500	-47.42775000	18.102	17.081	5813	3.78	0.97	-1.43	255.1	6.2
SGB_A.130	201.74654167	-47.42536111	18.109	17.059	5767	3.77	0.97	-1.32	225.4	6.2
SGB_A.135	201.68729167	-47.42155556	18.059	16.994	5652	3.70	0.99	-1.72	238.3	8.4
SGB_A.136	201.56879167	-47.42036111	18.050	16.955	5603	3.68	0.99	-1.63	225.5	8.0
SGB_A.138	201.70537500	-47.41897222	18.070	16.973	5588	3.68	0.99	-1.68	241.2	8.6
SGB_A.14	201.70050000	-47.54366667	18.073	17.028	5701	3.72	0.98	-1.71	229.4	8.2
SGB_A.141	201.61179167	-47.41819444	18.059	17.006	5708	3.72	0.98	-1.58	206.8	7.1
SGB_A.145	201.68179167	-47.41636111	18.148	17.145	5853	3.81	0.96	-1.45	244.4	6.4
SGB_A.146	201.63141667	-47.41597222	18.068	17.021	5748	3.74	0.98	-1.45	234.2	6.4

REFERENCES

Alonso, A., Arribas, S., & Martínez-Roger, C. 1999, A&AS, 140, 261

Bedin, L. R., Piotto, G., Anderson, J., Cassisi, S., King, I. R., Momany, Y., & Carraro, G. 2004, ApJ, 605, 125

Bedin, L. R., Cassisi, S., Castelli, F., Piotto, G., Anderson, J., Salaris, M., Momany, Y., & Pietrinferni, A. 2005, MNRAS, 357, 1038

Bellini, A., Piotto, G., Bedin, L. R., Anderson, J., Platais, I., Momany, Y., Moretti, A., Milone, A. P., & Ortolani, S. 2009, A&A, 493, 959

Blecha, A., Cayatte, V., North, P., Royer, F. & Simond, G. 2000, SPIE, 4008, 467

Cayrel, R. The impact of very high S/N spectroscopy on stellar physics, 132, 345

Calamida, A., Bono, G., Stetson, P. B., Freyhammer, L. M., Piersimoni, A. M., Buonanno, R., Caputo, F., Cassisi, S., Castellani, M., & Corsi, C. E. 2009, ApJ, 706, 1277

Cassisi, S., Salaris, M., Pietrinferni, A., Piotto, G., Milone, A.P., Bedin, L.,R., & Anderson, J. 2008, ApJ, 672, 115

D'Orazi, V., Gratton, R.G., Pancino, E., Bragaglia, A., Carretta, E., Lucatello, S., & Sneden, C. A&A, 2011, 534, 29

Gratton, R.G., Carretta, E., & Castelli, F.A&A, 314, 191

Gratton, R.G., Johnson, C.I., Lucatello, S., D'Orazi, V., & Pilachowski, C. 2011, A&A, 534, 72

Hilker, M., Kayser, A., Richtler, T., & Willemsen, P. 2004, A&A, 422, 9

Izzard, R. G., Tout, C. A., Karakas, A. I. & Pols, O. R. 2004, MNRAS, 350, 407

Johnson, C., & Pilachowski, C. A. 2010, ApJ, 722, 1373

Seok-Joo, Joo, & Young-Wook, Lee 2013, ApJ, 762, 36

King, I.R., Bedin, L.R., Cassisi, S., Milone, A.P., Bellini, A., Piotto, G., Anderson, J., Pietrinferni, A., & Cordier, D. 2012, AJ, 144, 5

Kurucz, R.L., Furenlid, I., Brault, J., & Testerman, L. 1984, Solar flux atlas from 296 to 1300 nm, National Solar Observatory Atlas, Sunspot, New Mexico: National Solar Observatory

Maeder, A. & Meynet, G 2006, A&A, 448, 37

Marino, A.F., Milone, A.P., Piotto, G., Villanova, S., Gratton, R., D'Antona, F., Anderson, J., Bedin, L.R., Bellini, A., Cassisi, S. 2011, ApJ, 731, 64

Marino, A.F., Milone, A.P., Piotto, G., Cassisi, S., D'Antona, F., Anderson, J., Aparicio, A., Bedin, L.R., Renzini, A., & Villanova, S. 2012, ApJ, 746, 14

Meylan, G. 2003, ASPC, 296, 17

Milone, A. P., Bedin, L. R., Piotto, G., Anderson, J., King, I. R., Sarajedini, A., Dotter, A., Chaboyer, B., Marín-Franch, A., Majewski, S. 2008, ApJ, 673, 241

Norris, J.E., Freeman, K.C., & Mighell, K.J. 1996, ApJ, 462, 241

Norris, J. E. 2004, ApJ, 612, 25

Pancino, E., Mucciarelli, A., Sbordone, L., Bellazzini, M., Pasquini, L., Monaco, L., & Ferraro, F. R. 2011, A&A, 527, 18

Pietrinferni, A., Cassisi, S., Salaris, M. & Castelli, F. 2006, ApJ, 642, 797

Piotto, G., Villanova, S., Bedin, L. R., Gratton, R., Cassisi, S., Momany, Y., Recio-Blanco, A., Lucatello, S., Anderson, J., King, I. R. 2005, ApJ, 621, 777

Reijns, R. A., Seitzer, P., Arnold, R., Freeman, K. C., Ingerson, T., van den Bosch, R. C. E., van de Ven, G., & de Zeeuw, P. T. 2006, A&A, 445, 503

Salaris, M., Chieffi, A. & Straniero, O. 1993, ApJ, 414, 580

Sivarani, T., Beers, T.C., Bonifacio, P., Molaro, P., Cayrel, R., Herwig, F., Spite, M., Spite, F., Plez, B., Andersen, J., Barbuy, B., Depagne, E., Hill, V., Francois, P., Nordstrom, B., & Primas, F. 2006, A&A, 459, 125

Sneden, C. 1973, ApJ, 184, 839

Sollima, A., Pancino, E., Ferraro, F. R., Bellazzini, M., Straniero, O., & Pasquini, L. 2005, ApJ, 634, 332

Stanford, L.M., Da Costa, G.S., Norris, J.E., & Cannon, R.D. 2006, ApJ, 647, 1075

Suntzeff, N.B., & Kraft, R.P. 1996, AJ, 111, 1913

van de Ven, G., van den Bosch, R. C. E., Verolme, E. K., & de Zeeuw, P. T. 2006, A&A, 445, 513

Villanova, S., Piotto, G., King, I. R., Anderson, J., Bedin, L. R., Gratton, R. G., Cassisi, S., Momany, Y., Bellini, A., Cool, A. M 2007, ApJ, 663, 296

Villanova, S., Geisler, D. & Piotto, G. 2010, ApJ, 722, 18

Villanova, S., & Geisler, D. 2011, A&A, 535, 31

Yong, D., Grundahl, F., Johnson, J. A. & Asplund, M. 2008, ApJ, 684, 1159

This 2-column preprint was prepared with the AAS LaTeX macros v5.2.